Revealing the Distribution of Metal Carboxylates in Oil Paint from the Micro- to Nanoscale

Xiao Ma, Victoria Beltran[+], Georg Ramer[+], Georges Pavlidis, Dilworth Y. Parkinson, Mathieu Thoury, Tyler Meldrum, Andrea Centrone, and Barbara H. Berrie**

Abstract: *Oil paints comprise pigments, drying oils, and additives that together confer desirable properties, but can react to form metal carboxylates (soaps) that may damage artworks over time. To obtain information on soap formation and aggregation, we introduce a new tapping-mode measurement paradigm for the photothermal induced resonance (PTIR) technique that enables nanoscale IR spectroscopy and imaging on highly heterogenous and rough paint thin sections. PTIR is used in combination with μ-computed tomography and IR microscopy to determine the distribution of metal carboxylates in a 23-year old oil paint of known formulation. Results show that heterogeneous agglomerates of Al-stearate and a Zn-carboxylate complex with Zn-stearate nano-aggregates in proximity are distributed randomly in the paint. The gradients of zinc carboxylates are unrelated to the Al-stearate distribution. These measurements open a new chemically sensitive nanoscale observation window on the distribution of metal soaps that can bring insights for understanding soap formation in oil paint.*

Oil paints have long been used to create artworks and find application as protective layers on wood or metals. They offer desirable aesthetic and physical characteristics. However, one common, typically ongoing reaction between metal ions (from metal-containing pigments) and free fatty acids (from hydrolyzed triglycerides of the oil binding medium and additives) leads to the formation of metal carboxylates (soaps). The formation of zinc and lead carboxylates appears to be a general process occurring in oil paints that lead to spalling, cracking, and the development of pimpled surfaces on artworks.[1] Metal soaps have also been identified in paints containing copper, cadmium, and manganese.[2] The physical deterioration caused by soap aggregation is a challenge for art conservation. Currently, much research[1b,3] is devoted to identifying the species involved and understanding the sequence of processes that lead to those adverse effects. For example, paint additives such as fats and metal stearates used to control paints' rheological properties and to promote pigment wetting can exacerbate soap formation by reacting with the pigments.[3d,4] However, not enough is known of soap formation and aggregation to mitigate their effects and propose effective conservation treatments.

In this work, we report a novel tapping-mode implementation scheme for the photothermal induced resonance (PTIR)[5] technique, a nano-infrared spectroscopy method that uses an atomic force microscope (AFM) probe to overcome the light diffraction limit. This new implementation, better adapted to measure highly heterogeneous and rough paint samples, is used here to study in detail the distribution of metal soaps in samples (hereafter paint outs) of known average composition prepared at the Grumbacher paint factory in 1995. Zinc-containing Pre-tested Soft Titanium White (P250) paint was chosen. This 23-year old, naturally-aged paint-out is completely analogous to an oil painting. It was chosen because it has not undergone any conservation treatment or artificial aging, thereby offering a well-characterized system for studying the development of soaps in real works of art.

PTIR reveals a complex distribution of metal carboxylates, which is heterogenous at the nanoscale. For example, it can detect three distinct metal carboxylates within and around a single agglomerate of the aluminum stearate additive. Since, as for most AFM techniques, PTIR has typically a low throughput, here synchrotron-based micro-computed tomography (μ-CT) and Fourier transform infrared (FTIR) micro spectroscopy are also employed to assess

[*] Dr. X. Ma, Dr. B. H. Berrie
Scientific Research Department, Division of Conservation
National Gallery of Art
2000B South Club Drive, Landover, MD 20785 (USA)
E-mail: B-BERRIE@nga.gov
Dr. V. Beltran,[+] Dr. M. Thoury
IPANEMA, CNRS, ministère de la Culture et de la Communication
Université de Versailles Saint-Quentin-en-Yvelines, USR 3461
Université Paris-Saclay
91128 Gif-sur-Yvette (France)
Dr. G. Ramer,[+] Dr. G. Pavlidis, Dr. A. Centrone
Nanoscale Device Characterization Division
Physical Measurement Laboratory
National Institute of Standards and Technology
100 Bureau Drive, Gaithersburg, MD 20899 (USA)
E-mail: andrea.centrone@nist.gov
Dr. G. Ramer[+]
Maryland Nanocenter, University of Maryland
College Park, MD 20742 (USA)
Dr. D. Y. Parkinson
Advanced Light Source, Lawrence Berkeley National Laboratory
1 Cyclotron Rd., Berkeley, CA 94720 (USA)
Prof. T. Meldrum
Department of Chemistry, William & Mary
540 Landrum Drive, Williamsburg, VA 23188 (USA)
[+] These authors contributed equally to this work.

compositional gradients across the whole paint film. Together these measurements offer new insights and further current efforts[6] to better understand soap formation and aggregation processes in artworks.

The initial nominal mass fractional composition of the paint (P250) is: drying oils (≈27 %), titanium white (anatase, ≈23 %), zinc white (≈46 %), and aluminum tristearate (Al-stearate, ≈4 %) added to counteract pigment settling in the paint tube and provide thixotropic behavior. The paint was applied as a ≈125 µm thick film onto a commercial zinc white oil-primed support, rather than an inert support. A cross-section sample of the paint-out (Figure 1 and Figure S1, Supporting Information) has 6 layers, labelled I to VI, whose composition was identified using a combination of analytical techniques confirming the expected formulation. See Supporting Information (Figure S1–S4) for the full characterization and further details of the components. Hereafter, we focus on the metal carboxylates, primarily in the paint layer VI.

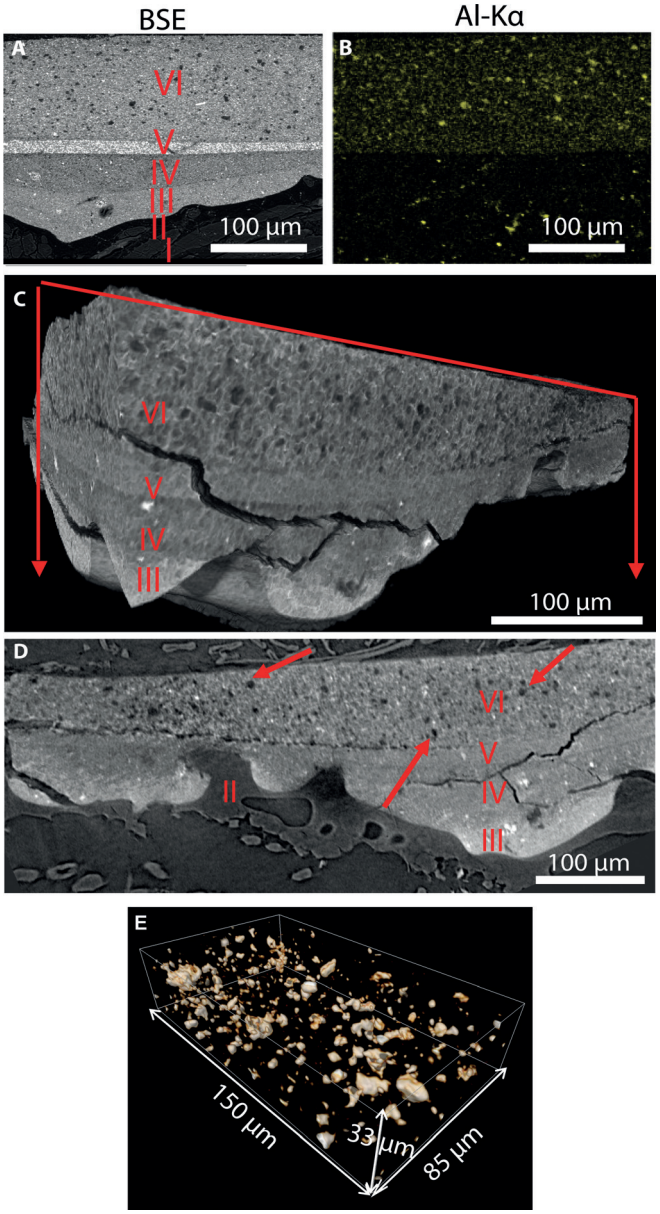

Figure 1. A) BSE image of P250, B) EDX map of Al, C–E) µ-CT analysis of P250, C) A grayscale map has been applied to show the range of linear absorption coefficients, D) a slice through the volume shown in (C) showing low density (dark) regions dispersed throughout the paint layer, E) 3D visualization of low-density regions in layer VI. Visualization was performed with volume rendering that shows higher X-ray absorbing materials transparent and lower absorbing materials opaque.

Transmission µ-FTIR spectra of powdered samples obtained from the priming layers III and IV and from the paint layer VI show similarities and notable differences (see Figure S5). In the priming layers III and IV, a broad band at ≈1590 cm^{-1} ν_{as} (COO^-) is like the broad peak of zinc soaps observed in nineteenth- and twentieth-century paintings.[3d,f,4a] This feature has been attributed to a mixture of zinc carboxylates with different molecular weights,[2] and a useful hypothesis suggests it is due to the formation of an ionomeric phase where zinc ions are an integrated part of a cured oil network that forms by metal ion migration and reaction with a oxidized linoxyn film.[3f] A broad carboxylate absorption also develops in model complexes obtained by reacting zinc acetate and ethyl linoleate, suggesting that soap formation in oil paint involves polyunsaturated fatty acids which, however, oxidize rapidly and are not present in historical paints.[7] Hereafter, we refer to this feature in the IR spectra as "zinc carboxylate". In the paint layer, peaks at 1540 cm^{-1} (ν_{as} (COO^-), sharp), 1464 cm^{-1} (δ (CH_2)) and 1398 cm^{-1} (ν_s (COO^-)) can be attributed to zinc stearate.[3b,e] The broad band centered at ≈1587 cm^{-1} derives from a small contribution of Al-stearate (ν_{as} (COO^-) ≈1588 cm^{-1}, a narrow peak) and from a large contribution of "zinc carboxylate" (ν_{as} (COO^-) ≈1590 cm^{-1}, a broad peak).

Hydrolysis of Al-stearate added to the paint leads to formation of free stearic acid which can react with zinc oxide to form zinc stearate ($ZnSt_2$).[3d,4a] Gabrieli et al. reported that large amounts of $ZnSt_2$ had formed in a mid-20th century oil painting due to the presence of Al-stearate.[4b] Below, we show that the distribution of zinc carboxylates in association with Al-stearate is more complex and heterogenous at the nanoscale than previously recognized.

Contrast in µ-CT images of an unembedded sample from P250 (Figure 1 C, D) shows low density (i.e., dark) regions dispersed throughout the paint film that correlate with low-atomic weight, Al-rich circular regions identified in the backscattered electron (BSE) image and Al-EDX map (Figure 1 A, B). Rotation of the µ-CT scan (Movie S1) reveals these regions are not spherical, but irregularly shaped, with lengths generally less than 10 µm (see 3D reconstruction in Figure 1 E). The distribution of absorption coefficients of the paint layer VI is plotted in Figure S6. Thresholding shows the Al-rich agglomerates are distributed randomly throughout the paint layer (Figure 1 D, E and Movie S2), meaning that cross sections and thin sections are representative of the paint film. No gradients, settling, or zoning of the Al-rich agglomerates are evident, in contrast to previous observations.[3d,4a] EDX analysis of a low-density agglomerate, on a ≈200 nm thick cross section (Figure S7), indicates that it contains both Al and Zn.

FTIR microscopy and PTIR nanoscopy were employed to investigate composition gradients and chemical heterogeneity in the paint film at the micro- and nanoscale, respectively. PTIR enables nanoscale IR characterization using an AFM probe as a near-field mechanical detector.[5] In PTIR, also known as AFM-IR, a pulsed wavelength-tunable laser illuminates a portion of the sample centered around the AFM tip. Following absorption of a light pulse, the sample heats and expands rapidly,[8] kicking the AFM cantilever into oscillation with an amplitude proportional to the absorbed energy.[9] The PTIR signal proportionality to the sample absorption coefficient, as in FTIR, enables identification of materials and chemical groups, leading to broad applications in materials science and biology.[8,10] Related to art conservation, PTIR was used to characterize parchment degradation[11] and the UV-induced, accelerated degradation of linseed oil in titanium white paints.[12] A key characteristic that distinguishes PTIR from other chemically-sensitive AFM techniques is its ability to probe the composition in samples even thicker than 1 µm.[13] Since the PTIR spatial resolution depends in part on the sample thermomechanical properties, the sample stratification and its thickness,[5,14] the best spatial resolution is obtained for thin (< 500 nm) samples that are vertically homogeneous. While PTIR experiments are typically carried out in contact-mode, here we employ tapping mode with a novel heterodyne detection scheme (Figure 2 A, B) where the tapping motion of the cantilever is mixed with the sample expansion due to non-linear tip-sample interactions.[15] Critically, this implementation is better adapted to analyze the chemically heterogeneous and topographically varied paint thin sections studied here. In particular, tapping-mode PTIR signal transduction is much less sensitive to heterogeneity in the sample mechanical properties than resonance-enhanced contact-mode operation.[6] In practice, a piezo actuator drives the cantilever at its second mechanical resonance ($f_2 \approx 1550$ kHz), the PTIR signal is demodulated at its first mechanical resonance ($f_1 \approx 250$ kHz) while pulsing the IR laser with a repetition rate $f_L = f_2 - f_1 \approx 1300$ kHz. With respect to our previous tapping-mode PTIR implementation[6,16] (signal demodulated at f_2), demodulating the signal at f_1, enables the acquisition of better quality tapping-mode PTIR spectra, which is key for chemical identification. This novel technical advance effectively broadens the PTIR application horizon to include samples that otherwise would be difficult to characterize in contact-mode, such as the samples relevant for paint degradation and other art conservation challenges.

PTIR maps and spectra (Figure 2) were obtained on a ≈200 nm thick section to identify the composition and the distribution of the Al-rich low-density agglomerates identified in Figure 1. Representative spectra (points 1–3, Figure 2 C, F) show that the agglomerate consists of Al-stearate (narrow peak at 1590 cm^{-1}), "zinc-carboxylate" (broad peak at ≈1590 cm^{-1}), oil (1742 cm^{-1}) and only a small amount of $ZnSt_2$ (shoulder at 1540 cm^{-1}). The large variation of the relative intensity of the 1590 cm^{-1} peak indicates that the proportion of Al-stearate within the agglomerate varies greatly. PTIR absorption maps at the above characteristic frequencies (marker bands) reveal the distribution of oil (Figure 2 E), "zinc carboxylate" plus Al-stearate (Figure 2 F) and $ZnSt_2$ (Figure 2 G). The latter shows nano-aggregates of

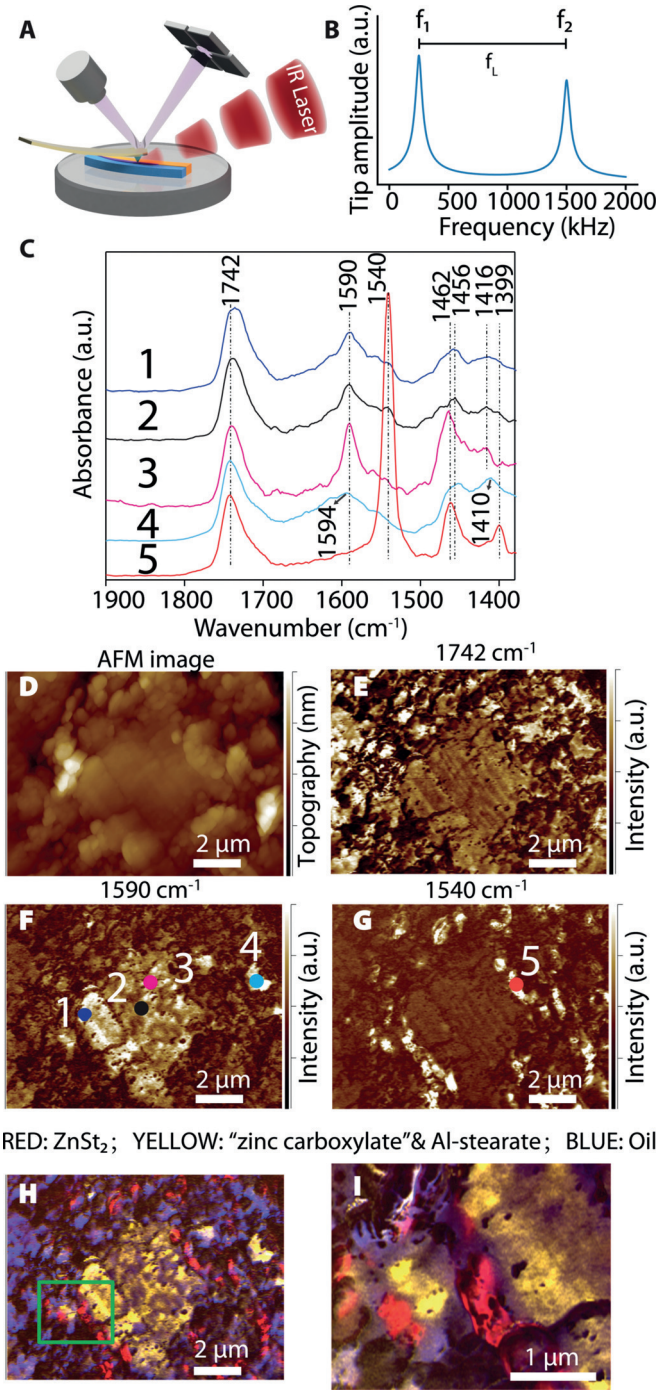

Figure 2. A) PTIR setup schematic, B) Tapping PTIR Scheme, C–I) PTIR analysis of a low-density region: C) PTIR spectra at the color-coded marked locations in (F) and (G) (points 1–5), the spectra were normalized to the ester band at 1742 cm^{-1} and offset for comparison, D) AFM topography. PTIR absorption maps at E) 1742 cm^{-1}, F) 1590 cm^{-1} and G) 1540 cm^{-1}, H) Reconstructed qualitative color-coded image of PTIR absorption intensity: $ZnSt_2$ (G, red), "zinc carboxylate" plus Al-stearate (F, yellow) and oil (E, blue). Colors are not displayed on a common intensity scale, I) Higher resolution image of the area delimited by the green box in H, see Figure S8 for original maps.

$ZnSt_2$ both at the rim of Al-rich agglomerate and in the paint film. The typical size of the $ZnSt_2$ clusters ranges from 100 nm to 400 nm, too small to be observed using μ-FTIR mapping.[4b] No concentration gradient of $ZnSt_2$ is observed at this scale. A representative spectrum from these areas (point 5, Figure 2C, G) shows strong 1540 cm^{-1} absorption ($ZnSt_2$, ν_{as} (COO^-)) and relatively weaker peak at 1742 cm^{-1} indicating a lower fraction of oil at that site. PTIR images overlaid (Figure 2H, I) show that the aluminum stearate-rich agglomerates and the nearest $ZnSt_2$ clusters are separated by a thin layer of oil. The likely explanation is that free stearic acid molecules migrate from the aluminum stearate-rich agglomerates through the oil to react with zinc oxide in the film.

The PTIR spectrum from an area with strong absorption at 1590 cm^{-1} outside the aluminum stearate-rich agglomerate (point 4, Figure 2C, F) has broad bands at ≈1594 cm^{-1} (ν_{as} (COO^-)) and 1410 cm^{-1} (ν_s (COO^-)) similar to those observed in real paintings[3d,4a] and in the priming layers (Figure S5). The phase characterized by this broad carboxylate peak derives from the reaction between zinc ions and oil. It is interesting to note this "zinc carboxylate" seems to be in localized areas and is not continuous throughout the paint film.

The high sensitivity and spatial resolution of PTIR allows disentangling the composition of paints and revealing for the first time that the agglomerates derived from the Al-stearate additive contain at least three metal carboxylates and oil. Unexpectedly, the zinc ions detected by EDX (Figure S7) belong mainly to "zinc carboxylate" (Figure 2C, F), demonstrating these species can intermix.

Although of lower spatial resolution, the higher measurement throughput of μ-FTIR mapping enables assessing the distribution and composition gradients in the whole paint film. Integrated absorption intensity maps of a thin section (6 μm) of the paint-out are shown in Figure S9. Notably, both $ZnSt_2$ (1540 cm^{-1}, Figure S9C) and "zinc carboxylate" (1587 cm^{-1}, Figure S9D) are present throughout the paint layer but with increasing concentration towards bottom and top of the layer, respectively. Deconvolution of the two carboxylate peaks in representative small areas (regions of interest—ROI 3 to 7 in Figure S9C) shows that the ratio of "zinc carboxylate"/$ZnSt_2$ peak area decreases gradually from the top of the film (ROI 3) to the bottom (ROI 7), see Figure 3 (inset Figure).

By normalizing the spectra from all ROIs to the CH_2 asymmetric stretching peak at ≈2918 cm^{-1} (Figure 3), two observations are possible. First, the ν_{as} (CH_2) at 2918 cm^{-1} (characteristic of aliphatic chains in *trans* conformation) shows a shoulder at ≈2926 cm^{-1} (characteristic of conformational disordered aliphatic chains)[17] that increases in intensity from the bottom to the top of the paint layer. Second, ν_{as} (CH_3) peak (≈2952 cm^{-1}) also increases in intensity from the bottom to the top of the paint film. This suggests that the aliphatic chains towards the top of the paint film are both shorter and more conformationally disordered, correlating well with the observed distribution of the "Zn carboxylate" phase.

The μ-FTIR spectrum of Grumbacher P250 expressed from a tube opened for the first time to perform the analysis

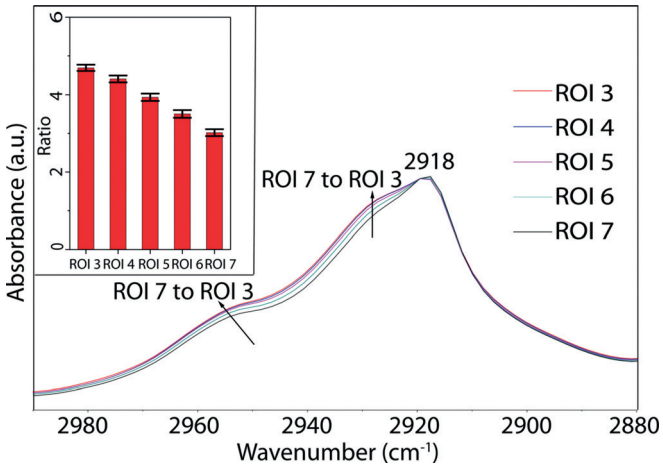

Figure 3. Spectra from ROI 3 to ROI 7 in the C–H stretching region normalized to the CH_2 asymmetric stretching at 2918 cm^{-1}. Inset Figure: ratio of the "zinc carboxylate"/ $ZnSt_2$ peak area. The error bars represent a single standard deviation in calculating the area ratio and were determined by propagating the uncertainty due to the deconvolution of the individual carboxylate peak areas.

(Figure S10) is similar to that of the cured paint layer (Figure S5) suggesting that $ZnSt_2$ and "zinc carboxylate" form inside the tube or even during the mixing process in the factory. The gradient in their relative concentrations in the cured paint film must, however, develop after the paint has been applied onto the canvas.

The development of $ZnSt_2$ gradients has been postulated to arise from $ZnSt_2$ migration towards[3d] or preferential formation at the bottom of paint films.[18] Although a gradient of $ZnSt_2$ is also observed in this work, no compelling evidence was obtained to distinguish between the two hypotheses. However, since the aluminum stearate-rich agglomerates are evenly distributed throughout the paint film, as shown from μ-CT, the zinc soaps gradients must form independently from Al-stearate. We hypothesize that from the top to the bottom of the paint film, the relative amount of free saturated fatty acids (contributing to $ZnSt_2$) increases with respect to the amount of polyunsaturated fatty acids and polymerized oil network (contributing to "zinc carboxylate").

The aged paint used in this study does not yet show signs of physical deterioration, however, we anticipate if hydrolysis of Al-stearate progresses, the concentration gradients of $ZnSt_2$ will become more pronounced, eventually leading to spalling.

The techniques used here provide chemical information over many length scales adding significantly to our knowledge of metal-carboxylate formation and distribution in paint. IR nanoscopy reveals for the first time that "zinc carboxylate" and Al-stearate are finely intermixed within aluminum stearate-rich agglomerates in oil paint. Additionally, $ZnSt_2$ nano-aggregates are found both near the rim of the aluminum stearate-rich agglomerates and dispersed throughout the paint. μ-FTIR mapping reveals expected $ZnSt_2$ and "zinc carboxylate" gradients. The findings are valuable for better understanding the relationship between the distribution of soaps and long-term changes in paint films that can ultimately

lead to paint deterioration. Particularly, the novel PTIR tapping-mode implementation presented here is better adapted to measure highly heterogeneous and topographically varying samples. Consequently, we believe that this PTIR measurement modality will find broad application in art conservation and for the characterization of a wider variety of material systems. The synergy of the methods used here can be applied broadly to address issues that challenge art conservation and other fields where materials with multiscale chemical heterogeneity are important, such as biomedicine and energy storage.

Acknowledgements

Xiao Ma was supported by a Charles E. Culpeper Advanced Fellowship at the National Gallery of Art. This research used resources of the Advanced Light Source, which is a DOE Office of Science User Facility under contract no. DE-AC02-05CH11231. Georg Ramer acknowledges support from the University of Maryland through the Cooperative Research Agreement between the University of Maryland and the National Institute of Standards and Technology Center for Nanoscale Science and Technology, Award 70NANB14H209. We thank Suzanne Lomax for performing GC/MS analysis and data interpretation, and Francesca Gabrieli for helpful discussions. The Grumbacher oil paint out is from the Art Materials Collection and Study Center at the National Gallery of Art.

[1] a) G. Osmond, K. Keune, J. Boon, *AICCM Bulletin* **2005**, *29*, 37; b) F. Casadio, K. Keune, P. Noble, A. V. Loon, E. Hendriks, S. A. Centeno, G. Osmond, *Metal Soaps in Art*, Springer, Dordrecht, **2019**.

[2] R. Mazzeo, S. Prati, M. Quaranta, E. Joseph, E. Kendix, M. Galeotti, *Anal. Bioanal. Chem.* **2008**, *392*, 65.

[3] a) J. J. Boon, J. van der Weerd, K. Keune, P. Noble, J. Wadum in *13th Triennial ICOM-CC Meeting*, *Vol. 1* (Ed.: R. Vontobel), James & James, Rio De Janeiro, **2002**, pp. 401; b) L. Robinet, M.-C. Corbeil, *Stud. Conserv.* **2003**, *48*, 23; c) C. A. Maines, D. Rogala, S. Lake, M. Mecklenburg, *MRS Proc.* **2011**, *1319*, mrsf10; d) G. Osmond, J. J. Boon, L. Puskar, J. Drennan, *Appl. Spectrosc.* **2012**, *66*, 1136; e) V. Otero, D. Sanches, C. Montagner, M. Vilarigues, L. Carlyle, J. A. Lopes, M. J. Melo, *J. Raman Spectrosc.* **2014**, *45*, 1197; f) J. J. Hermans, K. Keune, A. van Loon, P. D. Iedema, *J. Anal. At. Spectrom.* **2015**, *30*, 1600; g) J. Catalano, A. Murphy, Y. Yao, G. P. A. Yap, N. Zumbulyadis, S. A. Centeno, C. Dybowski, *Dalton Trans.* **2015**, *44*, 2340; h) Y.-c. K. Chen-Wiegart, J. Catalano, G. J. Williams, A. Murphy, Y. Yao, N. Zumbulyadis, S. A. Centeno, C. Dybowski, J. Thieme, *Sci. Rep.* **2017**, *7*, 11656; i) J. Catalano, A. Murphy, Y. Yao, N. Zumbulyadis, S. A. Centeno, C. Dybowski, *Solid State Nucl. Magn. Reson.* **2018**, *89*, 21.

[4] a) G. Osmond in *Issues in Contemporary Oil Paint* (Eds.: K. J. van den Berg, A. Burnstock, M. de Keijzer, J. Krueger, T. Learner, A. de Tagle, G. Heydenreich), Springer International Publishing, Cham, **2014**, pp. 263; b) F. Gabrieli, F. Rosi, A. Vichi, L. Cartechini, L. Pensabene Buemi, S. G. Kazarian, C. Miliani, *Anal. Chem.* **2017**, *89*, 1283.

[5] a) A. Centrone, *Annu. Rev. Anal. Chem.* **2015**, *8*, 101; b) A. Dazzi, C. B. Prater, *Chem. Rev.* **2017**, *117*, 5146.

[6] K. Wieland, G. Ramer, V. U. Weiss, G. Allmaier, B. Lendl, A. Centrone, *Nano Res.* **2019**, *12*, 197.

[7] M. G. MacDonald, M. R. Palmer, M. R. Suchomel, B. H. Berrie, *ACS Omega* **2016**, *1*, 344.

[8] J. Chae, S. An, G. Ramer, V. Stavila, G. Holland, Y. Yoon, A. A. Talin, M. Allendorf, V. A. Aksyuk, A. Centrone, *Nano Lett.* **2017**, *17*, 5587.

[9] A. Dazzi, F. Glotin, R. Carminati, *J. Appl. Phys.* **2010**, *107*, 124519.

[10] a) A. M. Katzenmeyer, J. Canivet, G. Holland, D. Farrusseng, A. Centrone, *Angew. Chem. Int. Ed.* **2014**, *53*, 2852; *Angew. Chem.* **2014**, *126*, 2896; b) J. Chae, Q. Dong, J. Huang, A. Centrone, *Nano Lett.* **2015**, *15*, 8114; c) S. Morsch, Y. Liu, S. B. Lyon, S. R. Gibbon, *ACS Appl. Mater. Interfaces* **2016**, *8*, 959; d) V. Giliberti, M. Badioli, A. Nucara, P. Calvani, E. Ritter, L. Puskar, E. F. Aziz, P. Hegemann, U. Schade, M. Ortolani, L. Baldassarre, *Small* **2017**, *13*, 1701181; e) G. Ramer, F. S. Ruggeri, A. Levin, T. P. J. Knowles, A. Centrone, *ACS Nano* **2018**, *12*, 6612.

[11] G. Latour, L. Robinet, A. Dazzi, F. Portier, A. Deniset-Besseau, M.-C. Schanne-Klein, *Sci. Rep.* **2016**, *6*, 26344.

[12] S. Morsch, B. A. van Driel, K. J. van den Berg, J. Dik, *ACS Appl. Mater. Interfaces* **2017**, *9*, 10169.

[13] B. Lahiri, G. Holland, A. Centrone, *Small* **2013**, *9*, 439.

[14] G. Ramer, V. A. Aksyuk, A. Centrone, *Anal. Chem.* **2017**, *89*, 13524.

[15] G. J. Verbiest, M. J. Rost, *Nat. Commun.* **2015**, *6*, 6444.

[16] M. Tuteja, M. Kang, C. Leal, A. Centrone, *Analyst* **2018**, *143*, 3808.

[17] a) R. G. Snyder, J. R. Scherer, B. P. Gaber, *Biochim. Biophys. Acta Biomembr.* **1980**, *601*, 47; b) A. Centrone, Y. Hu, A. M. Jackson, G. Zerbi, F. Stellacci, *Small* **2007**, *3*, 814.

[18] L. Baij, J. J. Hermans, K. Keune, P. Iedema, *Angew. Chem. Int. Ed.* **2018**, *57*, 7351; *Angew. Chem.* **2018**, *130*, 7473.